Photodetachment and photofragmentation pathways in the $[(CO_2)_2(H_2O)_m]^-$ cluster anions

Luis Velarde, Terefe Habteyes, and Andrei Sanov[a)]
Department of Chemistry, University of Arizona, Tucson, Arizona 85721-0041

(Received 22 June 2006; accepted 8 August 2006; published online 18 September 2006)

The mass-selected $[(CO_2)_2(H_2O)_m]^-$ cluster anions are studied using a combination of photoelectron imaging and photofragment mass spectroscopy at 355 nm. Photoelectron imaging studies are carried out on the mass-selected parent cluster anions in the $m=2-6$ size range; photofragmentation results are presented for $m=3-11$. While the photoelectron images suggest possible coexistence of the $CO_2^-(H_2O)_mCO_2$ and $(O_2CCO_2)^-(H_2O)_m$ parent cluster structures, particularly for $m=2$ and 3, only the CO_2^- based clusters are both required and sufficient to explain all fragmentation pathways for $m \geqslant 3$. Three types of anionic photofragments are observed: $CO_2^-(H_2O)_k$, $O^-(H_2O)_k$, and $CO_3^-(H_2O)_k$, $k \leqslant m$, with their yields varying depending on the parent cluster size. Of these, only $CO_2^-(H_2O)_k$ can potentially result from $(O_2CCO_2)^-(H_2O)_m$ parent structures, although an alternative mechanism, involving the dissociation and recombination of the CO_2^- cluster core, is possible as well. The $O^-(H_2O)_k$ and $CO_3^-(H_2O)_k$ channels are believed to be triggered by the dissociation of the CO_2^- cluster core. In the $CO_3^-(H_2O)_k$ channel, seen only in the range of $m=3-6$, the CO_2^- core dissociation is followed by an intracluster association of nascent O^- with the solvent CO_2. This channel's absence in larger clusters ($m>6$) is attributed to hindrance from the H_2O molecules.
 [DOI: 10.1063/1.2347707]

I. INTRODUCTION

Many known ionic clusters can be viewed as a charged core embedded in a "microsolution" consisting of a relatively small number of solvent molecules. This arrangement is helpful for studying reactions under well-defined microscopic conditions and understanding the structural motifs responsible for chemical reactivity.

Anionic clusters of carbon dioxide, in particular, have long been known to exhibit interesting structural properties.[1–13] The excess electron in homogeneous $(CO_2)_n^-$ either localizes on a single CO_2 (type-I clusters) or forms a covalent bond between two CO_2 monomers (type-II clusters), while the remaining molecules solvate the respective CO_2^- or $(O_2CCO_2)^-$ core anion.[5–8] Stepwise solvation normally results in a gradual increase of the cluster vertical detachment energy (VDE). On the contrary, the well-documented case of $(CO_2)_n^-$ is characterized by sharp discontinuities in VDE(n) between $n=6$ and 7 and again between $n=13$ and 14.[6,7] These discontinuities are attributed to "core switching" from $(O_2CCO_2)^-$ for $n<6$ to CO_2^- for $6<n<13$.[6] A reverse switch of the core anion structure back to $(O_2CCO_2)^-$ is observed for $n>13$.[7] Johnson and coworkers traced the origin of this phenomenon to the effect of solvent asymmetry.[8] Even though the most stable form of $(CO_2)_2^-$ corresponds to $(O_2CCO_2)^-$ rather than $CO_2^- \cdot CO_2$, an incomplete (asymmetric) solvation shell in the $n=6-13$ range causes one of the monomeric constituents of the dimer anion to be preferentially stabilized.[6–8,13] The photofragmentation of $(CO_2)_n^-$ was observed mainly in the $n>13$ range, yielding $(CO_2)_k^-$, $k<n$, fragment anions.[4] These fragmentation channels are presumably triggered either by the photodissociation of the $(O_2CCO_2)^-$ cluster core to $CO_2^-+CO_2$ or by photoinduced electron transfer to the solvent shell.

Heterogeneous clusters $[(CO_2)_n(H_2O)_m]^-$ present a more complex scenario, where the distinct molecular constituents, CO_2 and H_2O, may in principle compete for the excess electron. Photoelectron spectroscopy suggests that the charge remains localized on the carbon dioxide part of the cluster, either in a monomer or dimer configuration,[9,10,12,13] but the core switching follows a different trend, compared to $(CO_2)_n^-$.[12] A key feature of $[(CO_2)_n(H_2O)_m]^-$ observed in our group's imaging experiments is the loss of photodetachment anisotropy with increasing hydration.[12] We attributed this observation to autodetachment, but the exact nature of the excited states involved remained unclear.

An alternative route for excited-state dynamics is cluster fragmentation. Hence, the fragmentation studies are as important for understanding the cluster structure, particularly the nature of the excited states. The recent results for $CO_2^-(H_2O)_m$ contrasted the homogeneous anionic clusters of CO_2 in that one of the dominant pathways involved the dissociation of hydrated CO_2^- to O^-+CO.[14] The dissociation process can be understood in connection with the $^2\Pi_u$ shape resonance seen in dissociative electron attachment to CO_2 near 4.4 eV.[15–21] According to the proposed mechanism,[14] the 355 nm laser photon is absorbed by the CO_2^- cluster core, for which both the direct and indirect electron detachments are suppressed by the hydration interactions. The solvent-induced stabilization of the excited anion allows the bond dissociation to occur via a nonadiabatic bending process mediated by the Renner-Teller effect.

[a)]Electronic mail: sanov@u.arizona.edu

The nascent O^- formed in the dissociation of hydrated CO_2^- is expected to be highly reactive and clusters are a perfect environment to investigate its reactivity in detail. This premise motivates, in part, our present experiment, where we introduce an additional CO_2 in the hydrated cluster based on a CO_2^- core and observe its exothermic and barrierless reaction with nascent O^-. There have been few reports of reactions of nascent photofragments within anionic clusters.[4,22,23] The $O^- + CO_2 \rightarrow CO_3^-$ reaction was first observed in electron bombardment of van der Waals clusters of CO_2.[2,24,25] The CO_3^- peak in the electron attachment spectrum appears at 4.4 eV,[24] indicating that the attachment proceeds via the $^2\Pi_u$ resonance of CO_2. Alexander *et al.* ascribed a similar process to the minor CO_3^- channel in the fragmentation of $(CO_2)_n^-$, $6 < n < 13$.[4] Buntine *et al.* investigated the reaction of O^- with H_2O following the photodissociation of O_2^- within the $O_2^- \cdot H_2O$ complex at energies sufficient to overcome the reaction barrier.[23]

The addition of another CO_2 to $CO_2^-(H_2O)_m$ raises several questions. First, the nature of the ionic core of the new cluster must be determined. From the previous work, we anticipate the excess electron to reside on the CO_2 domain,[12] but whether the core of the cluster is a monomer or a dimer anion of CO_2 remains to be seen. Assuming the electron is on one CO_2, the competition of H_2O and the second (neutral) CO_2 for the binding sites in the proximity of the charged cluster core must be addressed. And most importantly, the $[(CO_2)_2(H_2O)_m]^-$ clusters allow the study of two types of photoinitiated reactions: the dissociation of a solvation-stabilized core and the secondary ion-molecule reaction of nascent photofragments with the solvent molecules.

In this work we utilize a combination of photoelectron imaging and photofragment mass spectroscopy to investigate the structure and reactivity of $[(CO_2)_2(H_2O)_m]^-$. The imaging experiments on the $m=2-6$ clusters expanded on our previous work[12] and shed light on the coexistence of the CO_2^- and $(O_2CCO_2)^-$ based species. The anionic fragmentation pathways observed by tandem time-of-flight mass spectroscopy for $m=3-11$ illuminate the reactivity of the clusters and provide further insights into the structure of their anionic cores.

II. EXPERIMENT

A schematic diagram of the experimental apparatus used in this work is shown in Fig. 1. This recently built instrument consists of a pulsed cluster-ion source and a tandem time-of-flight (TOF) mass spectrometer, employing the ion generation and mass analysis techniques pioneered by Lineberger and co-workers,[26,27] combined with a velocity-mapped[28] imaging[29] assembly for detection of photoelectrons. The ion source, primary TOF, and imaging parts of this apparatus are also similar to our first negative-ion machine described in detail elsewhere.[30,31]

Preparation of the $[(CO_2)_n(H_2O)_m]^-$ clusters involves expansion of undried CO_2 into the ion source chamber (base pressure of 2×10^{-7} Torr) through a pulsed supersonic nozzle (General Valve Series 99) operated at 3.5–4 atm stagnation pressure and a 50 Hz repetition rate. In addition to the

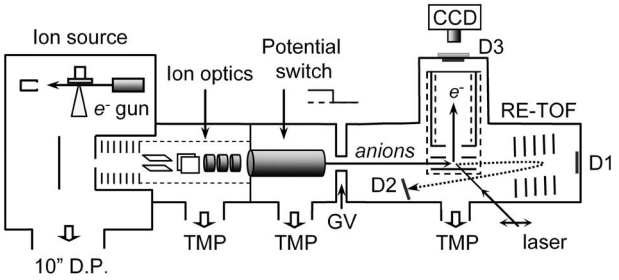

FIG. 1. Schematic diagram of the experimental apparatus. DP-diffusion pump, TMP-turbo-molecular pump, GV-gate valve, D1-in-line ion/neutral detector, D2-off-axis ion detector, and D3-photoelectron imaging detector. Double-headed arrow crossing the laser beam indicates the laser polarization direction.

CO_2 impurities, water trapped within the gas delivery lines serves as a source of H_2O. A continuous 1 keV electron beam crosses the free jet a few millimeters downstream from the 800 μm diameter valve orifice. The cluster anions are formed by secondary electron attachment to neutral clusters[26] and pulse extracted into a 2.3 m long flight tube of a Wiley-McLaren TOF mass spectrometer[32] by a transverse electric field (~1 kV/15 cm) applied approximately 18 cm downstream from the supersonic valve. The ions pass through a 4 mm diameter orifice in the grounded electrode separating the source chamber from the acceleration stack, where a uniform electric field from ten evenly spaced electrodes accelerates them to about 3 keV.

The accelerated ion beam is steered by two sets of electrostatic deflectors and focused using an Einzel lens. A fast potential switch[33] is used to reference the beam down to the ground potential without affecting its kinetic energy. In the detection region of the instrument (base pressure of 5×10^{-9} Torr), the ions are detected at the temporal and spatial foci of the mass spectrometer using an in-line microchannel plate (MCP) detector (Burle, Inc.) mounted at the end of the flight tube. The mass-selected ions are interrogated with a pulsed laser beam. The resulting ionic photofragments are analyzed with a single-field reflectron mass spectrometer, where the parent and assorted fragment ions are separated according to their mass. The reflectron assembly is tilted at 2.5° with respect to the primary TOF axis, deflecting the ions by 175° relative to the incoming beam velocity vector. The reflected fragments are detected by an off-axis MCP detector (Burle, Inc.) mounted at the spatial focus of the reflectron.

The third harmonic of a nanosecond Nd:YAG (yttrium aluminum garnet) laser (Spectra Physics, Inc., model Lab 130-50) is used in these experiments, providing 355 nm, 15 mJ pulses at a repetition rate of 50 Hz. The laser beam is brought to a 5 mm diameter spot at the intersection with the ion beam. Photoelectron images are recorded by collecting the electrons in a direction perpendicular to both the ion and the laser beams using a new imaging arrangement, which is similar to the one described previously.[34] The imaging MCP detector (Burle, Inc.) and the charge-coupled device (CCD) camera (Dalsa, Inc.) are operated in an event counting mode. Each image reported here represents 10 000–30 000 experimental cycles. The procedure for obtaining photofragment mass spectra is also described elsewhere.[26,35] In brief, the

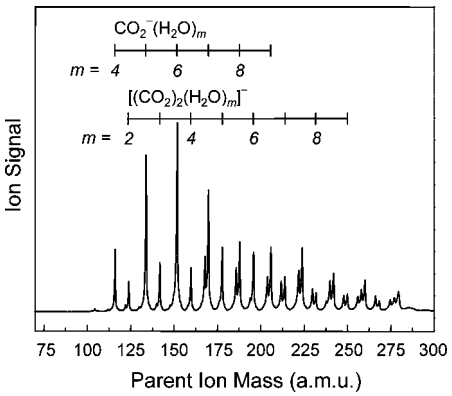

FIG. 2. Representative parent ion mass spectrum.

ionic fragments are collected by varying the potential on the reflectron to refocus the fragments of interest. The signals are averaged by the digitizing oscilloscope for 512 laser shots and then assembled into a combined mass spectrum representing all open fragmentation channels of the parent ion studied.

III. RESULTS AND ANALYSIS

A typical parent ion mass spectrum observed in this work is shown in Fig. 2. The most intense peak progression corresponds to the $CO_2^-(H_2O)_m$ cluster anions,[14] interspersed with less intense $[(CO_2)_2(H_2O)_m]^-$ peaks. Detectable but poorly resolved contributions of the $[(CO_2)_n(H_2O)_m]^-$, $n=3$ and 4, clusters are also seen. The formation of the $n=2$ cluster anions was optimized by adjusting the precursor gas backing pressure.

A. Photoelectron imaging

Figure 3 (left column) shows the photoelectron images of the $[(CO_2)_n(H_2O)_m]^-$, $m=2-6$, cluster anions collected at 355 nm. All images shown were recorded under the same velocity-mapping conditions. Similar to $CO_2^-(H_2O)_m$, $m=2-6$,[12] the $[(CO_2)_2(H_2O)_m]^-$, $m=2-6$, photoelectron images are anisotropic for small m, gradually becoming more isotropic as the number of H_2O's in the cluster increases. Here, we focus mainly on the photoelectron spectra, which are extracted from the images using the basis set expansion Abel-inversion algorithm of Dribinski *et al.*[36] The spectra are shown in the right column in Fig. 3. For $m=4-6$, the spectra contain one broad photoelectron band, while the $m=2$ spectrum includes two overlapping transitions. The $m=3$ spectrum exhibits a single maximum; nonetheless, the low electron kinetic energy (eKE) shoulder is suggestive of a second transition close to eKE=0.

We chose to characterize the photoelectron spectra in terms of the electron binding energy parameter, eBE_{max}, which corresponds to the eBE value for each observed band's maximum. For accurate determination of the peak positions, the individual photoelectron bands are modeled using the following profiles:

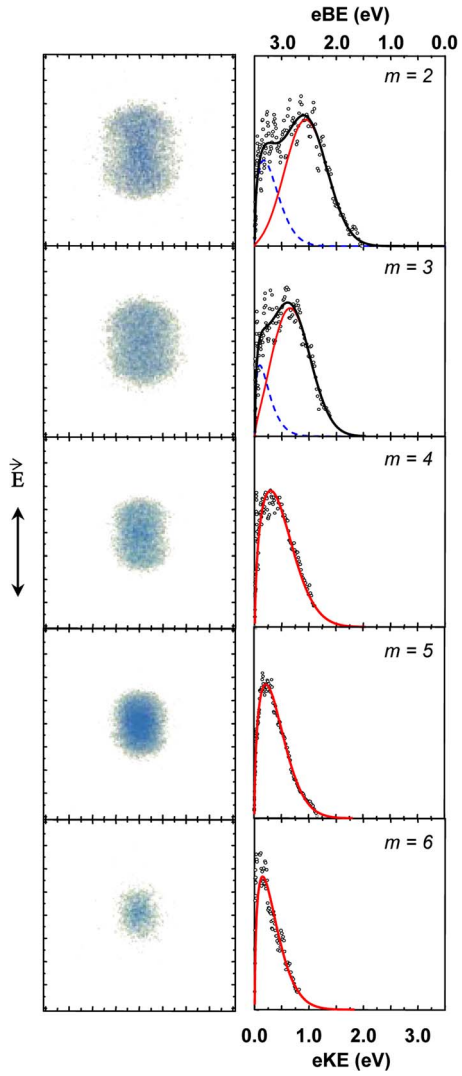

FIG. 3. (Color online) Photoelectron images (left) and corresponding photoelectron spectra (right) of the $[(CO_2)_2(H_2O)_m]^-$, $m=2-6$, cluster anions recorded at 355 nm. All photoelectron images are obtained under similar experimental conditions and shown to scale. The laser polarization direction is indicated by the double arrow on the left. In the right column, the experimental spectra are represented by open circles. The spectra are fitted by a sum (bold line) of contributions from type-I (solid) and type-II (dashed) parent clusters (see the text for details).

$$P(\mathrm{eKE}) = A\ \mathrm{eKE}^{1/2} \exp[-(h\nu - \mathrm{eKE} - \mathrm{VDE})^2/w^2]. \quad (1)$$

Here, $h\nu$ is the 355 nm photon energy (3.49 eV), VDE and w are the adjustable parameters corresponding to the vertical detachment energy and the Franck-Condon width of the bands, and A is a normalization factor.

The model function in Eq. (1) reflects the assumptions of the Franck-Condon model, within which the photodetachment cross section is given by $\sigma = Ch\nu v_e |\mathbf{M}_q|^2$, where v_e is the asymptotic electron velocity, $\mathbf{M}_q$ is the nuclear transition dipole moment, whose absolute value squared corresponds to the Franck-Condon factor, and C is a combination of fundamental constants.[37,38] The Gaussian function in Eq. (1) models the Franck-Condon envelope of the photodetachment transition, while $\mathrm{eKE}^{1/2}$ corresponds to the photoelectron velocity (speed).

At the fundamental level, the velocity factor in Eq. (1)

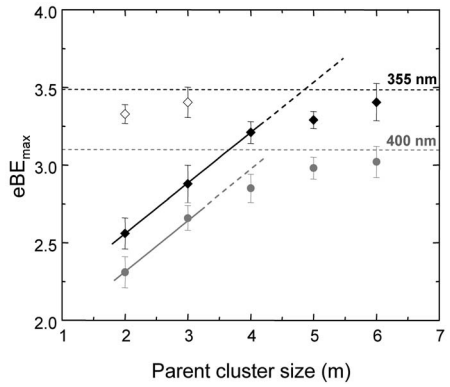

FIG. 4. The eBE_{max} values (defined in the text) for photoelectron bands arising from the dimer-based (open diamonds) and monomer-based (solid diamonds) $[(CO_2)_2(H_2O)_m]^-$ clusters at 355 nm. The corresponding values for $CO_2^-(H_2O)_m$ obtained at 400 nm (Ref. 12) are also shown for comparison (gray circles). Linear trends for $eBE_{max}(m)$ are indicated in the small m limit, where $eBE_{max} \approx$ VDE. The dashed horizontal lines indicate the 355 and 400 nm photon energies.

reflects the phase-space scaling of the number of the final free-electron states and also corresponds to the $\ell=0$ limit of the Wigner law for the photodetachment of negative ions.[39] In the photodetachment processes considered here, we expect contributions from partial waves with different ℓ values. The importance of the $\ell>0$ waves is particularly clear from the anisotropic nature of the photoelectron images in Fig. 3. Hence, the $eKE^{1/2}$ factor in Eq. (1) is approximate, but it suffices our goals, because the determination of eBE_{max} is not sensitive to the exact functional form of the model spectra, provided they yield a good agreement with the data.

The fits to the experimental spectra using Eq. (1) are shown in Fig. 3. For $m=2$ and 3, superpositions of two modified Gaussians with independently adjustable A, VDE, and w were used to achieve adequate agreement with the experiment. For $m=4-6$, one model function sufficed in each case. The values of eBE_{max} are determined at the maximum of each individual model band and the results are plotted as a function of m in Fig. 4. The eBE_{max} values are generally distinct from the corresponding VDEs: the former indicates the peak positions, while the latter corresponds to the maximum of the Franck-Condon envelope. Although the VDEs are often more relevant, their determination by spectral modeling may be strongly affected by the assumed scaling of the pre-Gaussian factor in Eq. (1), especially for bands with VDE$>h\nu$. For this reason, we use the peak positions (eBE_{max}) as a more robust way to characterize the spectra.

The eBE_{max} values represent the lower bounds for the corresponding VDEs. In the limit of $h\nu \gg$ VDE, the spectral bands peak near the corresponding VDE and therefore $eBE_{max} \approx$ VDE. When VDE nears the photon energy and particularly when $h\nu \leqslant$ VDE, the observed spectral maximum lies necessarily below the vertical transition energy, yielding $eBE_{max} <$ VDE. In Fig. 4, linear slopes of the $eBE_{max}(m)$ data are shown in the small m limit, where they reflect the stabilizing effect of hydration. As m increases, the corresponding eBE_{max} values level off, asymptotically approaching the photon energy. The two different 355 nm eBE_{max} values for $m=2$ and 3 correspond to two different modified-Gaussian

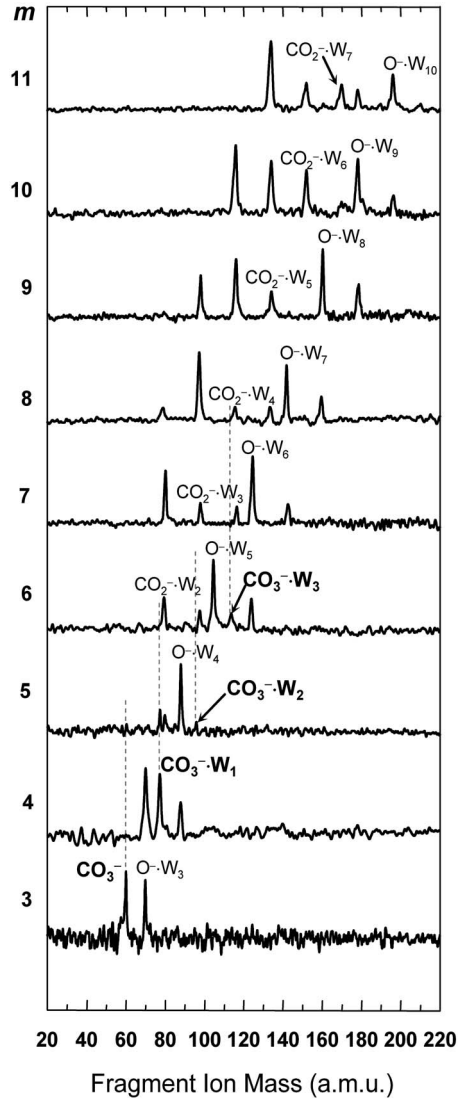

FIG. 5. Photofragment mass spectra obtained from $[(CO_2)_2(H_2O)_m]^-$, $m=3-11$, cluster anions at 355 nm. $W \equiv H_2O$.

bands used to model the corresponding photoelectron spectra in Fig. 3. Following the previous studies of carbon dioxide based cluster anions,[6,7,9,11] these bands are assigned to two different core anion structures.

B. Photofragment-ion mass spectra

The 355 nm photofragment mass spectra obtained for the mass-selected $[(CO_2)_2(H_2O)_m]^-$, $m=3-11$, parent ions are shown in Fig. 5 along with the assignment of the fragment-ion peaks. Only a very small CO_3^- signal was observed for the $m=2$ cluster, whose photodestruction is dominated by electron detachment. The fragmentation of $[(CO_2)_2(H_2O)_3]^-$ at 355 nm also occurs in acute competition with photodetachment, as evidenced by the relatively small yield of the anionic photofragments compared to total photodepletion. This is reflected in the poor signal-to-noise ratio of the $m=3$ spectrum in Fig. 5, compared to larger parent clusters. As the parent cluster size increases, the photodetachment becomes less energetically favorable, gradually giving way to the anionic fragmentation.

TABLE I. Anionic photofragments of mass-selected $[(CO_2)_2(H_2O)_m]^-$, $m=3-11$, parent clusters observed at 355 nm. The italicized values in parentheses represent the fractional yields of the corresponding fragments.

Parent size (m)	Photofragments		
	Type (i)	Type (ii)	Type (iii)
3	⋯	$O^-(H_2O)_3$ (*0.47*)	CO_3^- (0.53)
4	⋯	$O^-(H_2O)_3$ (*0.52*) $O^-(H_2O)_4$ (*0.13*)	$CO_3^-(H_2O)$ (*0.35*)
5	$CO_2^-(H_2O)_2$ (*0.15*)	$O^-(H_2O)_4$ (*0.64*)	$CO_3^-(H_2O)$ (*0.15*) $CO_3^-(H_2O)_2$ (*0.06*)
6	$CO_2^-(H_2O)_2$ (*0.18*) $CO_2^-(H_2O)_3$ (*0.10*)	$O^-(H_2O)_5$ (*0.45*) $O^-(H_2O)_6$ (*0.16*)	$CO_3^-(H_2O)_3$ (*0.11*)
7	$CO_2^-(H_2O)_2$ (*0.24*) $CO_2^-(H_2O)_3$ (*0.11*) $CO_2^-(H_2O)_4$ (*0.09*)	$O^-(H_2O)_6$ (*0.43*) $O^-(H_2O)_7$ (*0.14*)	⋯
8	$CO_2^-(H_2O)_2$ (*0.09*) $CO_2^-(H_2O)_3$ (*0.05*) $CO_2^-(H_2O)_4$ (*0.05*) $CO_2^-(H_2O)_5$ (*0.07*)	$O^-(H_2O)_7$ (*0.26*) $O^-(H_2O)_8$ (*0.15*)	⋯
9	$CO_2^-(H_2O)_3$ (*0.16*) $CO_2^-(H_2O)_4$ (*0.30*) $CO_2^-(H_2O)_5$ (*0.14*)	$O^-(H_2O)_7$ (*0.02*) $O^-(H_2O)_8$ (*0.24*) $O^-(H_2O)_9$ (*0.15*)	⋯
10	$CO_2^-(H_2O)_4$ (*0.29*) $CO_2^-(H_2O)_5$ (*0.21*) $CO_2^-(H_2O)_6$ (*0.17*) $CO_2^-(H_2O)_7$ (*0.04*)	$O^-(H_2O)_9$ (*0.22*) $O^-(H_2O)_{10}$ (*0.08*)	⋯
11	$CO_2^-(H_2O)_5$ (*0.41*) $CO_2^-(H_2O)_6$ (*0.13*) $CO_2^-(H_2O)_7$ (*0.16*)	$O^-(H_2O)_9$ (*0.09*) $O^-(H_2O)_{10}$ (*0.21*)	⋯

The spectra in Fig. 5 reveal three types of photofragments: (i) $CO_2^-(H_2O)_k$, (ii) $O^-(H_2O)_k$, and (iii) $CO_3^-(H_2O)_k$. Analogs of channels (i) and (ii), described as the evaporation and core-dissociation channels, respectively, were seen previously in $CO_2^-(H_2O)_m$.[14] Channel (iii) is new compared to $CO_2^-(H_2O)_m$ and is attributed to a sequential process: the dissociation of the CO_2^- cluster core to O^-+CO, followed by the association of nascent O^- with neutral CO_2 in the presence of H_2O. It is intriguing that type (iii) fragments appear only from the $m=3-6$ parent clusters. For comparison, only minor signatures of a similar process were seen previously in $(CO_2)_n^-$, $6 \leqslant n \leqslant 13$.[4,40]

The anionic photofragments resulting from the mass-selected parent clusters are summarized in Table I. The parent-size dependent fragmentation patterns are analyzed in terms of the fractional yields of individual photofragments, calculated by integrating the corresponding peak areas in the fragment mass spectra and normalizing the combined signal for a given parent size to unity. The resulting fractions are given in Table I in italics in parentheses.

IV. DISCUSSION

A. Charge localization in $[(CO_2)_2(H_2O)_m]^-$, $m=2-11$

The previous study of selected $[(CO_2)_n(H_2O)_m]^-$, $n=1-12$, $m=0-6$, cluster anions indicated that the excess electron in these clusters is localized on carbon dioxide.[12] The parent mass spectrum obtained in the present work is consistent with this conclusion. Indeed, the most intense progression in Fig. 2 corresponds to $[CO_2(H_2O)_m]^-$, followed by $[(CO_2)_2(H_2O)_m]^-$, while no hydrated electron clusters $(H_2O)_m^-$ are formed under the same experimental conditions. Hence, CO_2 appears to act as an electron binding site in the observed clusters.

This still leaves open two possibilities for charge localization in $[(CO_2)_2(H_2O)_m]^-$: the excess electron may be bound to a single CO_2 (type-I clusters) or shared between two CO_2 moieties (type-II clusters). It is well established that the most stable form of $(CO_2)_2^-$ is a type-II covalent dimer anion $(O_2CCO_2)^-$.[5,6] However, the core anion structure in clusters containing at least two CO_2 moieties varies from type I to type II depending on the balance between the stability of the core and solvation energetics. A prime example of such structural variation is the core switching phenomenon in $(CO_2)_n^-$.[6–8]

Of the $[(CO_2)_2(H_2O)_m]^-$ cluster anions, only the $m=2$ and 3 clusters were examined previously by photoelectron imaging at 400 nm.[12] The experiments indicated that the $m=2$ clusters have a major contribution from the $(O_2CCO_2)^-$ core type, which is followed by a switch to predominantly CO_2^- core structures for $m=3$. In the work reported here, the higher-energy 355 nm photons enabled us to image higher binding energy electrons and expand the measurements to larger clusters, containing up to six water molecules. The binding energies corresponding to the observed transition maxima, eBE_{max}, are plotted in Fig. 4. For $m=2$ and 3, two different eBE_{max} values are obtained, corresponding to two different photodetachment bands. These are attributed to the type-I (solid diamonds) and type-II (open diamonds) parent clusters, described as $CO_2^-(H_2O)_mCO_2$ and $(O_2CCO_2)^-(H_2O)_m$, respectively.

The assignment of the lower-eBE_{max} curve in Fig. 4 (solid diamonds) to type-I $CO_2^-(H_2O)_m$ CO_2 cluster anions is helped by comparison with the corresponding values obtained previously for $CO_2^-(H_2O)_m$, $m=2-6$, at 400 nm shown by gray circles.[12] Provided the eBE_{max} values are significantly smaller than the respective 355 or 400 nm photon energies, the type-I $[(CO_2)_2(H_2O)_m]^-$ and $CO_2^-(H_2O)_m$ trends are similar, shifted by approximately 0.2 eV, which corresponds to the stabilization by an extra CO_2 in the $[(CO_2)_2(H_2O)_m]^-$ case. The similar slopes of the two curves correspond to the stabilization energy of additional water molecules. We therefore interpret the $[(CO_2)_2(H_2O)_m]^-$ data indicated by solid diamonds as corresponding to $CO_2^-(H_2O)_mCO_2$ structures, where the additional CO_2 solvates the mostly unchanged $CO_2^-(H_2O)$ substructure.

The higher eBE_{max} values for the type-II $[(CO_2)_2(H_2O)_m]^-$, $m=2$ and 3, clusters are so close to the 3.49 eV photon energy that the corresponding VDEs are likely to be in excess of $h\nu$. With increasing m, the photodetachment of these clusters becomes energetically inaccessible at the laser wavelength used. Therefore, even though no type-II bands were used in modeling the $m \geqslant 4$ photoelectron

spectra in Fig. 3, we cannot completely rule out the presence of the type-II component in the parent cluster ion beam based on the photoelectron data alone.

Considering the fragmentation results in Sec. III B, we note that two of the three types of photofragment anions, namely, type (ii) $O^-(H_2O)_k$ and type (iii) $CO_3^-(H_2O)_k$, are inconsistent with type-II $(O_2CCO_2)^-(H_2O)_m$ parent structures. The $O^-(H_2O)_k$ channel in $(O_2CCO_2)^-(H_2O)_m$ is ruled out, because the dissociation of $(O_2CCO_2)^-$ is expected to first cleave its weakest (order of 1/2) C–C bond,[5] yielding the CO_2^- rather than O^- fragment anions. The CO_3^- channel in type-II clusters is even less plausible, as it would have to involve double dissociation of the $(O_2CCO_2)^-$ core to $O^- + CO + CO_2$, followed by an $O^- + CO_2 \rightarrow CO_3^-$ association. CO_3^- based products were previously seen in the photofragmentation of $(CO_2)_n^-$ cluster anions, in the $6 \leqslant n \leqslant 13$ size range only.[4,40] Later it was established that it is in this size range that the $(CO_2)_n^-$ cluster anions have CO_2^- cores (with the dimer and monomer core coexistence at $n=6,13$).[6–8] This parallel between the homogeneous and hydrated cluster results is another confirmation that the CO_3^- based fragments (in both cases) do indeed originate from parent clusters with CO_2^- cores.

Therefore, of all photofragments observed in this work, only the type (i) $CO_2^-(H_2O)_k$ photofragments can potentially arise from the type-II $(O_2CCO_2)^-(H_2O)_m$ parents. On the other hand, all three photofragment types are consistent with the type-I $CO_2^-(H_2O)_mCO_2$ clusters. Most notably, none of the photofragments for $m=3$ and 4 (see Table I) can be attributed to the type-II parents and hence the fragmentation of these clusters must be attributed to a type-I CO_2^- core.

In summary, the photofragmentation results overall point towards the type-I cluster anion structures described as $CO_2^-(H_2O)_mCO_2$, $m \geqslant 3$. This formula reflects the localization of the excess electron on a single CO_2 group, while the second, neutral CO_2 acts as a solvent. From the point of view of the energetics, the water molecules are expected to have priority in occupying the favorable binding sites in the first solvation shell around the core anion, which is reflected by placing the neutral CO_2 after the H_2O's. The preferential stabilization of the CO_2^- core by solvation of polar molecules was observed previously by Tsukuda *et al.*[9]

Photoelectron imaging, on the other hand, suggests the coexistence of type-I and type-II clusters for $m=2$ and 3. However, only the type-I clusters appear active in the photofragmentation, as no CO_2^- based fragments, expected from the type-II clusters, are seen. For $m>3$, the coexistence of the $CO_2^-(H_2O)_mCO_2$ and $(O_2CCO_2)^-(H_2O)_m$ structures remains possible and both may contribute to channel (i), yielding $CO_2^-(H_2O)_k$. However, just the CO_2^- based parent clusters are both required and sufficient to explain all the observed fragmentation pathways.

B. Solvent-evaporation and core-dissociation pathways in $[(CO_2)_2(H_2O)_m]^-$, $m=3-11$

As discussed in Sec. IV A, the type (i) fragments, $CO_2^-(H_2O)_k$, can be formed from either the type-I $CO_2^-(H_2O)_mCO_2$ or type-II $(O_2CCO_2)^-(H_2O)_m$ parent clusters. In the former case, these fragments should be described as solvent-evaporation products. In the latter, they result from the dissociation of the dimer-anion core.

The type (ii) $O^-(H_2O)_k$ fragment ions originate from the type-I clusters described as $CO_2^-(H_2O)_mCO_2$. The dissociation of the CO_2^- core has been proposed[14] to proceed via a solvent-enabled, Renner-Teller mediated mechanism and is followed by the ejection of CO from the cluster and evaporation of the solvent CO_2. The process may also involve the loss of one or, in rare cases, two H_2O molecules (see Fig. 5). For example, $CO_2^-(H_2O)_3CO_2$ yields only one type (ii) fragment, $O^-(H_2O)_3$, which corresponds to the loss of zero water molecules. On the other hand, the most intense $O^-(H_2O)_k$ fragments arising from $m=4-11$ reflect the loss of one H_2O.

C. Photoinduced ion-molecule reaction in $CO_2^-(H_2O)_mCO_2$, $m=3-6$, cluster anions

The appearance of the type (iii) $CO_3^-(H_2O)_k$, $k=0-3$, fragments for $m=3-6$ can be interpreted in terms of the following scheme:

$$CO_2^-(H_2O)_mCO_2 + h\nu \rightarrow (OC + O^-)(H_2O)_mCO_2 \quad (2a)$$

$$\rightarrow CO + CO_3^{-*}(H_2O)_m \quad (2b)$$

$$\rightarrow CO + CO_3^-(H_2O)_k + (m-k)H_2O. \quad (2c)$$

Here, the fragmentation process is initiated by the dissociation of the CO_2^- cluster core [Eq. (2a)] via the Renner-Teller mediated mechanism discussed previously[14] and in Sec. IV B. Considering the relatively small parent cluster size ($m=3-6$), the CO fragment is likely to be ejected from the cluster before the loss of any solvent molecules can occur. The O^- fragment, on the other hand, is bound to the remainder of the cluster by stronger ion-neutral interactions and may trigger a barrierless ion-molecule association reaction with the solvent CO_2 [Eq. (2b)]. The water molecules act as an energy-absorbing bath, stabilizing the CO_3^- product at the expense of evaporation of several H_2O's [Eq. (2c)].

The dissociation energy of CO_3^- to $O^- + CO_2$ in the absence of a solvent was recently determined to be 2.79 eV (64.34 kcal/mol).[41] This accounts for the bulk of the total energy dissipated by water evaporation in Eq. (2c). In addition, the kinetic energy of nascent O^- arising from the dissociation of CO_2^- should be considered, but is expected to be comparatively small. This is specially true since a significant fraction of the CO_2^- dissociation excess energy is deposited into the CO counterfragment, as indicated by the studies of dissociative electron attachment to CO_2.[17,19] Yet another factor affecting the reaction energetics is the effect of hydration, particularly the difference in the hydration energies of the parent, intermediate, and product ions: CO_2^-, O^-, and CO_3^-, respectively. Viggiano *et al.*[42] reported $\Delta H \leqslant -25$ kcal/mol for the reaction of monohydrated O^- with CO_2. Without providing a lower bound for the ΔH, this estimate differs significantly from the isolated-reaction exothermicity quoted above. Roehl *et al.*[43] assigned a value of 1.58 eV (36.4 kcal/mol) to the energy difference between the

$O^-(H_2O)+CO_2$ products and the $CO_3^-(H_2O)$ parent ion. In the absence of more thermodynamic data for the reaction of $O^-(H_2O)_m$ with CO_2, Yang and Castleman made use of the expected similarities with reactions of $OH^-(H_2O)_n$ with CO_2 to predict that the enthalpy change approaches nearly a constant value as the cluster size increases.[44]

These uncertainties make evaluating the intracluster $O^-+CO_2 \rightarrow CO_3^-$ reaction energetics rather difficult. From the above ΔH values,[42,43,45] we estimate that the energy dissipated by water evaporation in Eq. (2c) should be in the range of 30–40 kcal/mol (1.3–1.7 eV). Keesee *et al.*[46] reported enthalpies corresponding to the $CO_3^-(H_2O)_m \rightarrow CO_3^-(H_2O)_{m-1}+H_2O$ reactions to range from 14.1 kcal/mol (0.61 eV) for $m=1$ to 13.1 kcal/mol (0.57 eV) for $m=3$. Hence, in the $m=3-6$ range, where the $CO_3^-(H_2O)_k$ fragments are seen, the assumed reaction exothermicity is expected to be sufficient for evaporating about three water molecules. This estimate agrees with the experimental results, as most $CO_3^-(H_2O)_k$ fragments correspond to the loss of three H_2O's. Should these products be interpreted as electrostatically bound $O^-\cdot CO_2$ or $O^-(H_2O)_kCO_2$ complexes, the energy required for the observed water loss would be lacking. Hence, the observed evaporation is a signature of the formation of a new chemical bond in the CO_3^- based products.

The critical step of the above mechanism, the association of O^- with CO_2 in the presence of water molecules, has been studied separately.[42,44] Viggiano *et al.* examined the reactions of $O^-(H_2O)_{1,2}$ with CO_2 and observed CO_3^- as the only ionic product.[42] Yang and Castleman[44] studied the reactions of larger hydrated clusters of O^- with CO_2 and proposed a mechanism, according to which the $O^-(H_2O)_m$ clusters react with CO_2 via ligand substitution. In this process, the thermodynamically favored association yields a new cluster core, while the immediate evaporation of a ligand (solvent) removes some of the reaction exothermicity.

Finally, the possibility of intracluster reaction of the nascent O^- fragments with H_2O giving OH^-+OH needs to be addressed. Buntine *et al.* characterized this reaction following the photodissociation of O_2^- within the $O_2^-\cdot H_2O$ complex.[23] In the present work, we observe no sign of this reaction, which is not surprising considering that the process is endothermic by 0.36 eV.[47] Without accounting for the hydration effects, only an estimated 0.1 eV is released in 355 nm dissociation of CO_2^-. This value is obtained as the difference between $h\nu$ and the bond dissociation energy, calculated as $D_0(CO-O^-)=D_0(CO-O)-AEA(O)+AEA(CO_2)$, where $D_0(CO-O)=5.453$ eV is the corresponding value for $CO_2 \rightarrow CO+O(^3P)$,[48,49] and $AEA(O)=1.461$ eV and $AEA(CO_2)=-0.6$ eV are the adiabatic electron affinities of $O(^3P)$ (Ref. 50) and CO_2,[51] respectively. For comparison, in the $O_2^-\cdot H_2O$ experiment of Buntine *et al.* the nascent O^- fragments carried recoil energies of up to 0.75 eV.[23]

D. Channel competition

Both the $O^-(H_2O)_k$ and $CO_3^-(H_2O)_k$ fragment channels are triggered by the photodissociation of the CO_2^- core of the parent $CO_2^-(H_2O)_mCO_2$ cluster. It is therefore intriguing that the relative yield of the ion-molecule reaction products, $CO_3^-(H_2O)_k$, decreases with m in the $m=3-6$ range and no fragments of this type are observed for $m>6$. As evident in Fig. 5, in the $m=7-11$ clusters *the second, neutral* CO_2 *molecule is always lost* in the fragmentation process.

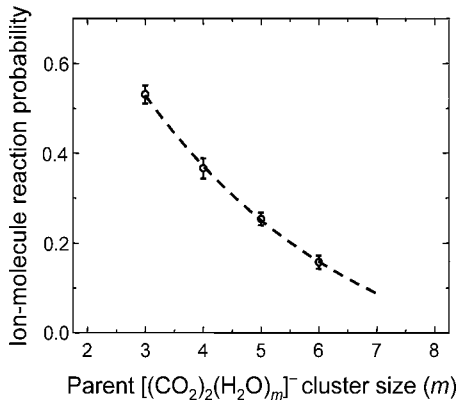

FIG. 6. Probability for the nascent O^- fragment to undergo an intracluster ion-molecule association reaction with CO_2.

To quantify this observation, we define the probability for the core dissociation [Eq. (2a)] to lead to a successful association reaction of nascent O^- with the solvent CO_2 [Eqs. (2b) and (2c)] as follows:

$$\phi_{IM}(m)=\frac{I(CO_3^-)}{I(O^-)+I(CO_3^-)}. \tag{3}$$

Here, $I(CO_3^-)$ and $I(O^-)$ represent the integrated intensities of all $O^-(H_2O)_k$ and $CO_3^-(H_2O)_k$ fragments, respectively, observed for a given m. Hence, the denominator accounts for all channels involving the dissociation of the CO_2^- cluster core, while the numerator represents the secondary ion-molecule reaction events. The fraction $\phi_{IM}(m)$ is plotted in Fig. 6, indicating that the probability of the nascent O^- reaction with CO_2 decreases rapidly with increasing hydration. Previously, Viggiano *et al.*,[42] independently followed by Yang and Castleman,[44] also found a reduction in reactivity with increasing hydration.

This decrease in the secondary ion-molecule reaction probability may be indicative of the neutral CO_2 being physically separated from the CO_2^- cluster core (and therefore the nascent O^-) by the water molecules. This hypothesis is consistent with the expectation that the water molecules will tend to have priority (over CO_2) in occupying the binding sites in the immediate proximity of the ionic core.

V. SUMMARY

The fragmentation of mass-selected $[(CO_2)_2(H_2O)_m]^-$, $m=3-11$, cluster anions points towards predominantly CO_2^- based parent structures, described as $CO_2^-(H_2O)_mCO_2$. Photoelectron spectroscopy, however, suggests the coexistence of the $CO_2^-(H_2O)_mCO_2$ and $(O_2CCO_2)^-(H_2O)_m$ structures for $m=2-3$ and some presence of the $(O_2CCO_2)^-$ based clusters cannot be ruled out for larger clusters ($m>3$) as well. Nonetheless, just the CO_2^- based structures are required and sufficient to explain all the observed photofragmentation pathways.

Three types of anionic photofragments are observed at 355 nm: $CO_2^-(H_2O)_k$, $O^-(H_2O)_k$, and $CO_3^-(H_2O)_k$, $k \leqslant m$. The $O^-(H_2O)_k$ and $CO_3^-(H_2O)_k$ channels are believed to be triggered by the dissociation of the CO_2^- cluster core. In the $CO_3^-(H_2O)_k$ channel, the dissociation is followed by an intracluster reaction of nascent O^- with the solvent CO_2, yielding a CO_3^- anion, which is stabilized by interactions with the water molecules. This channel is seen only in the parent cluster size range of $m=3-6$, where its relative yield decreases rapidly with increasing m. This behavior is attributed to a decrease in the probability of the secondary ion-molecule reaction of nascent O^- with CO_2 due to hindrance from H_2O. Some ambiguity remains regarding the mechanism for the $CO_2^-(H_2O)_k$ channel. The possibilities include the dissociation of the CO_2^- cluster core followed by its recombination,[14] as well as the dissociation of the $(O_2CCO_2)^-$ core to $CO_2^-+CO_2$.

ACKNOWLEDGMENTS

This work is supported by the NSF Grant No. CHE-0134631 and the Packard Fellowship in Science and Engineering.

[1] C. E. Klots and R. N. Compton, J. Chem. Phys. **67**, 1779 (1977).
[2] C. E. Klots and R. N. Compton, J. Chem. Phys. **69**, 1636 (1978).
[3] C. E. Klots, J. Chem. Phys. **71**, 4172 (1979).
[4] M. L. Alexander, M. A. Johnson, N. E. Levinger, and W. C. Lineberger, Phys. Rev. Lett. **57**, 976 (1986).
[5] S. H. Fleischman and K. D. Jordan, J. Phys. Chem. **91**, 1300 (1987).
[6] M. J. DeLuca, B. Niu, and M. A. Johnson, J. Chem. Phys. **88**, 5857 (1988).
[7] T. Tsukuda, M. A. Johnson, and T. Nagata, Chem. Phys. Lett. **268**, 429 (1997).
[8] J. W. Shin, N. I. Hammer, M. A. Johnson, H. Schneider, A. Gloss, and J. M. Weber, J. Phys. Chem. A **109**, 3146 (2005).
[9] T. Tsukuda,M. Saeki, R. Kimura, and T. Nagata, J. Chem. Phys. **110**, 7846 (1999).
[10] M. Saeki, T. Tsukuda, S. Iwata, and T. Nagata, J. Chem. Phys. **111**, 6333 (1999).
[11] R. Mabbs, E. Surber, L. Velarde, and A. Sanov, J. Chem. Phys. **120**, 5148 (2004).
[12] E. Surber, R. Mabbs, T. Habteyes, and A. Sanov, J. Phys. Chem. A **109**, 4452 (2005).
[13] A. Muraoka, Y. Inokuchi, N. Nishi, and T. Nagata, J. Chem. Phys. **122**, 094303 (2005).
[14] T. Habteyes, L. Velarde, and A. Sanov, Chem. Phys. Lett. **424**, 268 (2006).
[15] M. J. W. Boness and G. J. Schulz, Phys. Rev. Lett. **21**, 1031 (1968).
[16] G. J. Schulz and D. Spence, Phys. Rev. Lett. **22**, 47 (1969).
[17] C. R. Claydon, G. A. Segal, and H. S. Taylor, J. Chem. Phys. **52**, 3387 (1970).
[18] O. J. Orient and S. K. Srivastava, Chem. Phys. Lett. **96**, 681 (1983).
[19] P. J. Chantry, J. Chem. Phys. **57**, 3180 (1972).
[20] A. Stamatovic and G. J. Schulz, Phys. Rev. A **7**, 589 (1973).
[21] R. Dressler and M. Allan, Chem. Phys. **92**, 449 (1985).
[22] V. Vorsa, Ph.D. thesis, University of Colorado, 1996.
[23] M. A. Buntine, D. J. Lavrich, C. E. Dessent, M. G. Scarton, and M. A. Johnson, Chem. Phys. Lett. **216**, 471 (1993).
[24] A. Stamatovic, K. Leiter, W. Ritter, K. Stephan, and T. D. Mark, J. Chem. Phys. **83**, 2942 (1985).
[25] A. Stamatovic, K. Stephan, and T. D. Mark, Int. J. Mass Spectrom. Ion Process. **63**, 37 (1985).
[26] M. A. Johnson and W. C. Lineberger, in *Techniques for the Study of Ion Molecule Reactions*, edited by J. M. Farrar and W. H. Saunders (Wiley, New York, 1988), p.591.
[27] M. E. Nadal, P. D. Kleiber, and W. C. Lineberger, J. Chem. Phys. **105**, 504 (1996).
[28] A. T. J. B. Eppink and D. H. Parker, Rev. Sci. Instrum. **68**, 3477 (1997).
[29] D. W. Chandler and P. L. Houston, J. Chem. Phys. **87**, 1445 (1987).
[30] E. Surber, S. P. Ananthavel, and A. Sanov, J. Chem. Phys. **116**, 1920 (2002).
[31] R. Mabbs, E. Surber, and A. Sanov, Analyst (Cambridge, U.K.) **128**, 765 (2003).
[32] W. C. Wiley and I. H. McLaren, Rev. Sci. Instrum. **26**, 1150 (1955).
[33] L. A. Posey, M. J. DeLuca, and M. A. Johnson, Chem. Phys. Lett. **131**, 170 (1986).
[34] E. Surber, R. Mabbs, and A. Sanov, J. Phys. Chem. A **107**, 8215 (2003).
[35] M. L. Alexander, N. E. Levinger, M. A. Johnson, D. Ray, and W. C. Lineberger, J. Chem. Phys. **88**, 6200 (1988).
[36] V. Dribinski, A. Ossadtchi, V. A. Mandelshtam, and H. Reisler, Rev. Sci. Instrum. **73**, 2634 (2002).
[37] H. Massey, *Negative Ions*, 3rd ed. (Cambridge University Press, Cambridge, 1976).
[38] K. M. Ervin and W. C. Lineberger, in *Advances in Gas Phase Ion Chemistry*, edited by N. G. Adams and L. M. Babcock (JAI, Greenwich, 1992), Vol. 1, p. 121.
[39] E. P. Wigner, Phys. Rev. **73**, 1002 (1948).
[40] M. L. Alexander, Ph.D. thesis, University of Colorado, 1987.
[41] J. C. Bopp, E. G. Diken, J. M. Headrick, J. R. Roscioli, and M. A. Johnson, J. Chem. Phys. **124**, 174302 (2006).
[42] A. A. Viggiano, R. A. Morris, C. A. Deakyne, F. Dale, and J. F. Paulson, J. Phys. Chem. **94**, 8193 (1990).
[43] C. M. Roehl, J. T. Snodgrass, C. A. Deakyne, and M. T. Bowers, J. Chem. Phys. **94**, 6546 (1991).
[44] X. Yang and A. W. Castleman, J. Am. Chem. Soc. **113**, 6766 (1991).
[45] R. G. Keesee and A. W. Castleman, J. Phys. Chem. Ref. Data **15**, 1011 (1986).
[46] R. G. Keesee, N. Lee, and A. W. Castleman, J. Am. Chem. Soc. **101**, 2599 (1979).
[47] C. Lifshitz, J. Phys. Chem. **86**, 3634 (1982).
[48] D. R. Harding, R. E. Weston, and G. W. Flynn, J. Chem. Phys. **88**, 3590 (1988).
[49] M. C. Lin and S. H. Bauer, J. Chem. Phys. **50**, 3377 (1969).
[50] C. Valli, C. Blondel, and C. Delsart, Phys. Rev. A **59**, 3809 (1999).
[51] R. N. Compton, P. W. Reinhardt, and C. D. Cooper, J. Chem. Phys. **63**, 3821 (1975).